Peak effects in the kagome superconductors CsV_3Sb_5 and $Cs(V_{0.93}Nb_{0.07})_3Sb_5$

Chunlei Wang ,[1,2] Yuki Hirota,[1] Lubin Wang,[2] Ryosuke Sakagami ,[1] Yongkai Li,[3,4] Xiaolei Yi,[2] Wenjie Li ,[1] Yangsong Chen,[1] Cheng Yu,[1] Zhiwei Wang,[3,4,*] and Tsuyoshi Tamegai [1,†]

[1]*Department of Applied Physics, The University of Tokyo, Tokyo 113-8656, Japan*
[2]*Department of Physics and Electronic Engineering, Xinyang Normal University, Xinyang 464000, China*
[3]*Centre for Quantum Physics, Key Laboratory of Advanced Optoelectronic Quantum Architecture and Measurement (MOE), School of Physics, and Beijing Key Lab of Nanophotonics and Ultrafine Optoelectronic Systems, Beijing Institute of Technology, Beijing 100081, China*
[4]*Material Science Center, Yangtze Delta Region Academy of Beijing Institute of Technology, Jiaxing 314011, China*

(Received 7 October 2023; revised 28 December 2023; accepted 9 January 2024; published 29 January 2024)

The effect of 3 MeV proton irradiation on the superconductivity of CsV_3Sb_5 and $Cs(V_{0.93}Nb_{0.07})_3Sb_5$ has been investigated by resistivity and magnetization measurements. The critical transition temperature T_c increases from 3.2 to 4.4 K after proton irradiation for CsV_3Sb_5 single crystals. Besides the enhanced critical current density, we observe a broad magnetization peak in the proton-irradiated CsV_3Sb_5 single crystals, which can be attributed to the enhancement of vortex pinning induced by irradiation. We find the magnetization peak close to the upper critical field H_{c2} in $Cs(V_{0.93}Nb_{0.07})_3Sb_5$ single crystals, which should come from the softening of the flux line lattice. The T_c is slightly suppressed after proton irradiation in $Cs(V_{0.93}Nb_{0.07})_3Sb_5$ single crystals at the present irradiation doses. The vortex phase diagrams have been constructed for the kagome superconductors $Cs(V_{0.93}Nb_{0.07})_3Sb_5$ and proton-irradiated CsV_3Sb_5 based on the obtained data.

DOI: 10.1103/PhysRevB.109.024514

I. INTRODUCTION

Coexistence and competition between superconductivity and density wave orders are often observed in novel superconductors such as cuprate [1,2], iron-based [3,4], and heavy Fermion [5,6] superconductors; this has become one of the hottest topics in condensed matter physics in recent years. The kagome lattice, composed of corner-sharing triangles and hexagons, provides a versatile platform for investigating fascinating quantum phenomena. Recently, kagome compounds AV_3Sb_5 ($A = K$, Rb, Cs), which possess nontrivial band topology such as Dirac points and saddle points, were discovered to exhibit some novel properties including possible chiral charge-density wave (CDW), anomalous Hall effect (AHE), and unconventional superconductivity [7–14]. Application of pressure or chemical doping can suppress the CDW order, but enhance the superconductivity. For example, the superconductivity exhibits a two-dome-like behavior under moderate pressure, while the CDW order is monotonically suppressed by pressure, indicating an unusual competition between the superconductivity and the CDW order [10,15–19]. It has been reported that Nb substitution for V in CsV_3Sb_5 can also enlarge T_c up to about 4.45 K with the suppression of CDW transition temperature from about 92 to 58 K [20]. The hole-doped samples, such as $CsV_{3-x}Ti_xSb_5$ and $CsVsSb_{5-x}Sn_x$, were found to have two superconducting domes and a completely suppressed CDW transition [21–23].

To investigate the superconductivity in some superconductors with competing CDW order, one effective method is to introduce artificial defects by irradiation [24,25]. Compared with chemical doping, light particle irradiation can introduce pointlike defects and avoid changes in the charge carrier density and Fermi surface topology [26,27]. In general, the artificial defects introduced by irradiation suppress the superconductivity due to the pair-breaking effect [28]. However, the enhanced T_c has been observed after ion irradiation in some superconductors with competing orders [29,30]. In addition, the depairing current density in these systems is about $J_d \sim 10^7$ A/cm^2, which is comparable to MgB_2 or $Ba_{1-x}K_xFe_2As_2$. However, values of critical current density J_c in CsV_3Sb_5 and Ta-doped CsV_3Sb_5 are only about $\sim 3 \times 10^3$ and 2×10^4 A/cm^2 at 1.8 K and self-field, respectively, which are far less than those of MgB_2 or $Ba_{1-x}K_xFe_2As_2$ [31–34]. One of the possible reasons for this difference is that the systems lack effective pinning centers. It is expected the flux pinning potential will be enhanced after high-energy particle irradiation.

In this paper, we investigate the changes of superconductivity in CsV_3Sb_5 and $Cs(V_{0.93}Nb_{0.07})_3Sb_5$ after 3 MeV proton (H^+) irradiation. We observe the enhancement of T_c from 3.2 to 4.4 K for CsV_3Sb_5 after proton irradiation with a dose of 0.1×10^{16} ions/cm^2, and the T_c is suppressed slowly with further increase in irradiation dose. A broad magnetization peak has been observed in a CsV_3Sb_5 single crystal after proton irradiation. For a $Cs(V_{0.93}Nb_{0.07})_3Sb_5$ single crystal, there is a clear peak effect at fields close to the upper critical field H_{c2}, which has been attributed to the order to disorder transition of flux line lattice [35–37]. After proton irradiation, the T_c of $Cs(V_{0.93}Nb_{0.07})_3Sb_5$ monotonically decreases with

*zhiweiwang@bit.edu.cn
†tamegai@ap.t.u-tokyo.ac.jp

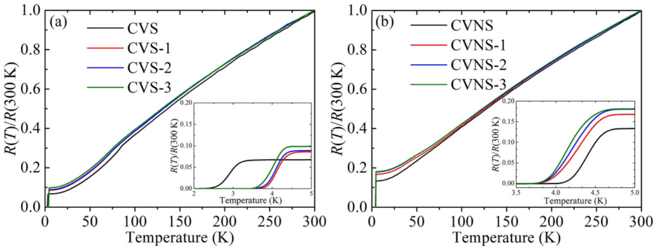

FIG. 1. Temperature dependence of normalized resistance $R(T)/R(300\,\mathrm{K})$ for (a) CsV_3Sb_5 and (b) $Cs(V_{0.93}Nb_{0.07})_3Sb_5$ with and without proton irradiation. Insets: the corresponding blowups of superconducting transition at temperatures close to T_c.

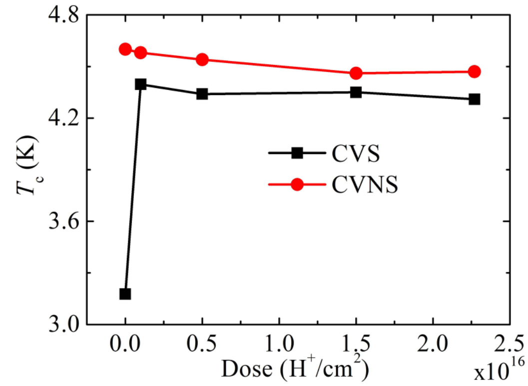

FIG. 2. Irradiation dose dependence of T_c for CVS and CVNS.

increasing irradiation dose. The mechanism of vortex pinning and the phase diagram of the vortex for $Cs(V_{0.93}Nb_{0.07})_3Sb_5$ and proton-irradiated CsV_3Sb_5 crystals are proposed based on the obtained experimental data.

II. EXPERIMENTAL METHODS

Single crystals of CsV_3Sb_5 and Nb-doped $Cs(V_{1-x}Nb_x)_3Sb_5$ (with $x = 0.07$) were grown by the self-flux method, which has been reported elsewhere [20]. All the proton-irradiated samples were cleaved into thin flakes with thickness less than 15 μm. This value is smaller than the projected range of a 3 MeV proton for the CsV_3Sb_5 system of $\sim 57\,\mu\mathrm{m}$ [38]. The 3 MeV proton irradiation experiments were conducted at NIRS-HIMAC in Chiba, Japan. The samples are irradiated at 100 K in vacuum less than 1×10^{-5} Torr. The irradiation dose of the proton is controlled by measuring the total charge of the proton deposited into the sample holder with a known distribution of the beam profile. For convenience, the pristine single crystals of CsV_3Sb_5 and $Cs(V_{0.93}Nb_{0.07})_3Sb_5$ are named CVS and CVNS, and the corresponding proton irradiated samples for both kinds of crystals with doses of 0.1×10^{16}, 0.5×10^{16}, and $2.3 \times 10^{16}\,\mathrm{ions/cm^2}$ are called CVS-1, CVS-2, and CVS-3, and CVNS-1, CVNS-2, and CVNS-3, respectively. The standard four-probe method was employed to measure the resistivity. The measurements of resistivity and magnetization are carried out on DynaCool-PPMS-9T system and SQUID magnetometer (MPMS-XL5, Quantum Design).

III. RESULTS AND DISCUSSION

Figures 1(a) and 1(b) show the normalized resistance $[R(T)/R(300\,\mathrm{K})]$ versus temperature curves for CVS and CVNS, respectively, before and after proton irradiation. For CVS, the CDW transition temperature (T^*) is about 87 K which is slightly lower than 95 K as reported in Ref. [11]. The value of RRR (residual resistance ratio) is about 15.4, which is smaller than that (RRR = 84) reported in Ref. [25] indicating that much stronger impurity scattering is present in our CVS crystals [25]. One of the possible reasons is that there are many more atomic-sized defects introduced during the fabrication of crystals. After proton irradiation, the values of $R(5\text{ K})/R(300\text{ K})$ increase due to the enhanced scattering by defects [39,40]. For CVS, the onset superconducting critical transition temperature (T_c) is about 3.2 K with a transition width $\sim$0.6 K. After proton irradiation, the CDW transition becomes weak even with a small dose of $0.1 \times 10^{16}\,\mathrm{ions/cm^2}$. This phenomenon suggests that the CDW transition is suppressed by the proton irradiation. In contrast to the suppressed CDW transition, the T_c is enhanced after the irradiation for CsV_3Sb_5. For example, the onset T_c is boosted up to about 4.4 K for CVS-1. It is well known that there is a delicate competition between the superconductivity and CDW order in the CsV_3Sb_5 system. Extensive experimental studies, including the techniques of doping and high pressure, reveal the fact that the superconductivity is enhanced by the suppression of CDW order [15,20]. One reasonable explanation is that different parts of the Fermi surface are respectively in charge of superconductivity and CDW order. Chemical doping, irradiation, and high pressure destabilize CDW order and recover the Fermi surface to be utilized by superconductivity. Recently, Roppongi *et al.* investigated the effect of electron irradiation on the properties of CsV_3Sb_5. They found that both T_c and CDW transition of CsV_3Sb_5 are suppressed after 2.5 MeV electron irradiation [25]. It is difficult to explain their results based on the competition between superconductivity and CDW order. Furthermore, the additional scattering of electrons due to defects created by electron irradiation should be temperature independent. Thus it is reasonable to observe parallel shift in ρ-T curves after electron irradiation. However, the ρ-T curves after electron irradiation show obvious temperature-dependent behavior in their samples. All these facts are confusing and require more experiments to verify them. In the sample studied in the present study, the T_c decreases slightly with further increase in the irradiation doses; for example, the T_c drops down to about 4.34 and 4.30 K for the samples of CVS-2 and CVS-3, respectively, as shown in Fig. 1(a). This behavior of T_c is analogous to that of $NbSe_2$ single crystals, where the T_c is initially enhanced from 7.2 K up to 7.5 K, followed by monotonic suppression by successive 2.5 MeV electron irradiations [29]. In the case of CVNS, the CDW transition is suppressed greatly. The T_c for CVNS is about 4.6 K, which is suppressed weakly to about 4.57, 4.54, and 4.47 K for samples of CVNS-1, CVNS-2, and CVNS-3, respectively, as shown in Fig. 1(b). Except for the initial increase of T_c at a small dose accompanied by the suppression of CDW in CVS-1, all the data suggest weak dependence of T_c on the dose of irradiation as shown in Fig. 2. These results suggest that CVS and CVNS are *s*-wave

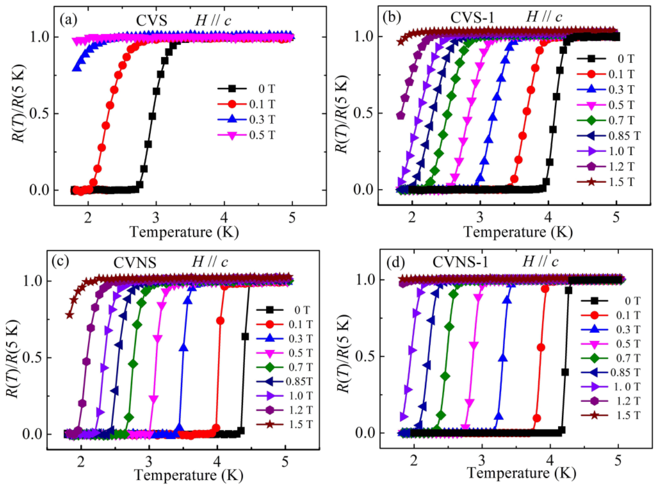

FIG. 3. Temperature dependence of normalized resistivity $R(T)/R(5\,\mathrm{K})$ under different magnetic fields for (a) CVS, (b) CVS-1, (c) CVNS, and (d) CVNS-1.

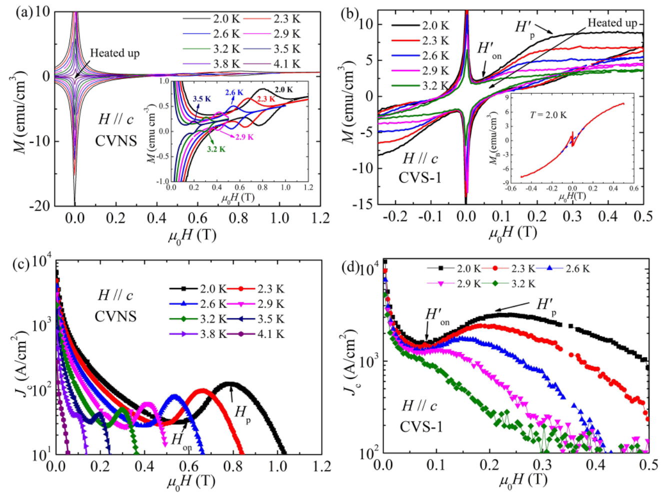

FIG. 4. The MHLs for (a) CVNS and (b) CVS-1. The inset of (a) shows blowups of the peak effect. The corresponding J_c-H curves for (c) CVNS and (d) CVS-1. The inset of (b) shows the magnetic field dependence of background magnetization (M_B) after proton irradiation for CVS-1. Below $|\mu_0 H| < 0.08\,\mathrm{T}$, M_B is contaminated by the superconducting signal, and the expected value is shown by the blue dotted line.

superconductors, which is consistent with the results reported in Refs. [16,22,41].

Figures 3(a)–3(d) show the temperature dependence of resistance under different magnetic fields ($H//c$) for the CVS, CVS-1, CVNS, and CVNS-1, respectively. It can be seen that the critical transition temperature for CVS is very sensitive to the applied magnetic field, and the superconductivity is almost completely suppressed below 1.8 K at 0.5 T as shown in Fig. 3(a). Figure 3(b) displays the temperature dependence of normalized resistance under different fields from 0.1 to 1.5 T for CVS-1. After proton irradiation, the superconductivity of CVS has been obviously improved, and a clear superconducting transition above 1.8 K can be observed even at a high magnetic field of 1.2 T. The superconductivity in CVNS is the most robust among them, and we can observe a complete superconducting transition above 1.8 K even at 1.2 T as shown in Fig. 3(c). However, the superconductivity decays after proton irradiation and the resistance cannot get down to zero above 1.8 K even at 1.0 T as shown in Fig. 3(d). The temperature dependences of normalized resistance for CVS-2, CVS-3, CVNS-2, and CVNS-3 are shown in Fig. S1 in the Supplemental Material [42]. For all the samples, the onset and zero resistance temperatures are suppressed with increasing magnetic field, and the transition width stays nearly constant, which is similar to that of low-T_c conventional superconductors, "'122" and "1144" iron-based superconductors [31,43], but clearly different from high-T_c cuprate, iron-based "1111" and "11111" type superconductors [44–46]. We can evaluate the values of upper critical field H_{c2} by using the criterion of the resistance transition of $0.5R_n$, where R_n is the normal state resistance just above T_c. According to the Ginzburg-Landau (GL) equation, $H_{c2}(T) = H_{c2}(0)(1–t^2)/(1 + t^2)$, where $t(= T/T_c)$ is the reduced temperature. The evaluated values of $H_{c2}(0)$ for CVS, CVNS, CVS-1, and CVNS-1 are about 0.8, 1.9, 1.6, 1.65 T, respectively, and the corresponding coherence lengths $\xi(0)$ are evaluated to be about 20.2, 13.5, 14.4, and 14.1 nm, respectively, based on the formula of $\xi(0) = (\Phi_0/2\pi H_{c2})^{1/2}$. These values are consistent with those reported in Ref. [47].

The magnetization hysteresis loops (MHLs) for CVNS and CVS-1 are shown in Figs. 4(a) and 4(b), respectively. For CVNS, the symmetric curves indicate that the bulk pinning instead of the surface pinning dominates flux pinning in the sample. In addition, the MHL curve for a pristine CVS measured at a temperature of 2 K shown in Fig. S2(a) [42] also gives a very symmetric pattern. Li *et al.* have investigated the MHL curves for CsV_3Sb_5 and Ta-doped CsV_3Sb_5 single crystals, which show asymmetric curves [34]. These results indicate that superconducting properties of CVS and doped CVS sensitively depend on the details of growth conditions. However, the widths of the MHL curves are also very small in the present samples suggesting that vortex pinning is very weak. As mentioned above, the current CVS single crystals may have more point defects related to their smaller value of RRR. In general, these defects play roles as pinning centers and enhance the critical current density. However, we have not observed any significant enhancement in MHL curves in the CVS specimen. One of the possible reasons is that the dimensions of the defects are much smaller than the coherence length, leading to negligible pinning force to vortices. It is interesting to observe a sharp peak effect close to H_{c2} in CVNS as shown in the inset of Fig. 4(a). It should be pointed out that the peak effect becomes weak after proton irradiation in CVNS. For example, only a very small magnetization peak close to H_{c2} is observed at 2 K for CVNS after proton irradiation at a very small dose of $0.05 \times 10^{16}\,\mathrm{ions/cm^2}$ as shown in Fig. S2(b) [42]. As is well known, the proton irradiation introduces point pinning centers, and vortices can be pinned by them, resulting in the formation of very disordered vortex lattice at low temperatures. Thus, it is reasonable to observe a very weak magnetization peak on top of enhanced irreversible magnetization after irradiation. Recently, STM (scanning tunneling microscopy) studies have revealed that

CsV_3Sb_5 single crystals possess a well-arranged triangular vortex lattice just like that observed in 2*H*-$NbSe_2$ [47]. Thus it is expected to have a similar peak effect induced by softening of the vortex lattice. However, the MHL curve obtained at 2 K shows no such peak effects, as shown in Fig. S2(a) [42]. One possible reason is that the measuring temperature ~ 2 K is too close to T_c so that the peak effect shifts to low fields and merges with the peak at the self-field. Recently, Zhang *et al.* observed a similar peak effect in CsV_3Sb_5 using the ac mutual inductance technique down to lower temperatures [48]. The J_c's calculated based on the Bean model for CVNS specimens are shown in Fig. 4(c), and the corresponding peak effect can be clearly seen in the J_c-H curves at different applied fields. The value of J_c is about 0.65×10^4 A/cm^2 at 2 K and the self-field, and this small J_c indicates that vortex pinning in CVNS is weak [47]. It should be pointed out that the main assumption of the Bean model is that the superconducting current flows with a field-independent critical current density (J_c) in regions of a superconductor where local induction is changed. Such current causes the field-dependent penetration of vortices and size-dependent magnetization. The onset, H_{on}, and the peak of the peak effect, H_p, are determined by the criterion of $dJ_c/dH = 0$, which defines local minimum and maximum in J_c-H curves, as shown in the inset of Fig. 6(a). It can be seen that both H_{on} and H_p increase with decreasing temperature. The width of the peak effect, which is defined by $\Delta H = H_p - H_{on}$, slowly decreases with increasing temperature. For example, ΔH is ~ 0.09 T ($H_{on} \sim 0.32$ T and and $H_p \sim 0.41$ T) at 2.9 K, while ΔH is ~ 0.04 T ($H_{on} \sim 0.155$ T and $H_p \sim 0.195$ T) at 3.5 K. These phenomena remind us of the similar peak effect observed in 2*H*-$NbSe_2$, which has been attributed to the order-disorder transition accompanied by the softening of the vortex lattice [35,49]. In addition, we also calculate the magnetic relaxation ratio based on the formula of $Q = d\ln(\Delta M)/d\ln(dH/dt)$ and the typical result is shown in Fig. S3 [42]. It can be seen that Q decreases sharply at the region of the peak effect, supporting the idea of abrupt softening of the vortex lattice. The self-energy of vortices per unit length can be evaluated by $E_{sf} = \Phi_0^2 \ln\kappa/4\pi\mu_0\lambda^2$, where Φ_0 is the flux quantum and κ is equal to λ/ξ. It can be seen that the evaluated values of E_{sf} for CVNS are comparable to that of Nb_3Sn [50]. In other words, vortices in CVNS are rigid. As a result, vortices cannot occupy energetically favorable positions due to large elastic moduli. However, the situation will change when the applied magnetic field is close to H_{c2} and the full value of the pinning force can be obtained due to the softening of the vortex lattice, leading to a sharp peak in the MHL and J_c-H curves just before falling to zero at H_{c2} [51].

On the other hand, broad enhancements of J_c at intermediate fields are observed in CVS-1 as shown in Fig. 4(d). With increasing temperature, the peak moves to low fields and the magnitude of the peak becomes small. A similar broad peak effect is also observed in CVS-2 samples as shown in Fig. S4 [42]. It should be pointed out that the peak effect in CVS-2 is weaker than CVS-1, which can be attributed to the damaging of superconductivity under a larger irradiation dose together with the reduced T_c. It should be noted that magnetic backgrounds appear in CVS and CVNS after proton irradiation as shown in the inset of Fig. 4(b) and

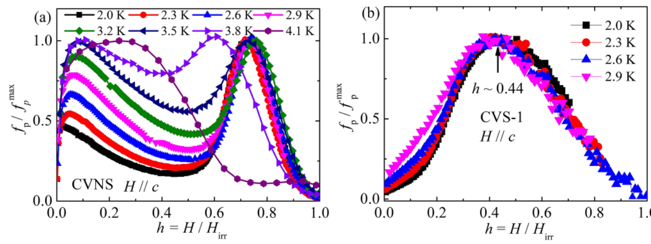

FIG. 5. The relationship between normalized pinning force density (F_p) and reduced magnetic field (h) for (a) CVNS and (b) CVS-1 single crystals.

Fig. S5 [42]. The magnetic background is evaluated according to the formula $M_B = (M^+ + M^-)/2$, where $M^+(M^-)$ is the magnetization for increasing (decreasing) field. Whether such magnetic background is generated right after the introduction of defects or a combined effect of defects and their growths after exposure to air needs to be clarified in the future. The field dependence of J_c is also calculated according to the Bean model, and the corresponding values of J_c at different temperatures are shown in Fig. 4(d). The value of J_c is about 1.2×10^4 A/cm^2 at 2 K and at the self-field for CVS-1, and this value is close to that in Ta-doped CsV_3Sb_5 single crystals [47]. The H'_{on} and H'_p are also defined as the local minimum and maximum in the J_c-H curves with the same criterion of $dJ_c/dH = 0$ for the CVS-1 samples. It can be seen that the H'_p moves to lower magnetic fields while H'_{on} stays nearly constant with increasing temperature. As a result, the interval between H'_{on} and H'_p becomes less with increasing temperature. For example, H'_p at 2.0 and 2.9 K are ~ 0.22 and ~ 0.11 T, and the corresponding H'_{on} is $\sim$0.08 and $\sim$0.07 T, respectively. Thus the widths $\Delta H'$ ($= H'_p - H'_{on}$) decrease from $\sim$0.14 to $\sim$0.04 T by increasing temperature from 2.0 to 2.9 K. The monotonic suppression of H'_p with increasing temperature is similar to that observed in cuprate and iron-based superconductors, which suggests that all of them may have similar mechanisms [52–55].

In order to investigate the pinning mechanism of vortices related to the peak effect in CVNS and CVS-1, the pinning force density is calculated based on the formula of $f_p = \mu_0 H \times J_c$. Figures 5(a) and 5(b) show dependence of the normalized pinning force density [$F_p(h) = f_p(h)/f_p^{max}$] on the reduced field $h = H/H_{irr}$ for CVNS and CVS-1, respectively. The value of H_{irr} is obtained from the J_c-H curves with the criterion of 10 A/cm^2. For CVNS, the $F_p(h)$ curves show two peaks locating at low and high fields, respectively. The position of the peak at low fields is very close to zero in the present temperature range. For example, the corresponding values of h for the peak are about 0.016 and 0.08 at 2 and 3.5 K, respectively, as shown in Fig. 5(a). According to the Dew-Hughes theory, the pinning force $f_p(h)$ should be proportional to $h^p(1-h)^q$. For bulk pinning, the values of p and q are 0 and 2, respectively, with a peak located at $h = 0$. Thus the mechanism of flux pinning at low fields is mainly bulk pinning for CVNS. At high fields, there is another peak close to H_{c2}, which is caused by the order-disorder transition of vortices, just like that observed in $NbSe_2$, $Ba_{1-x}K_xBiO_3$, and $YBa_2Cu_3O_{7-\delta}$ [35–37]. At temperatures very close to

T_c, for example, at $T = 3.8$ and 4.1 K, H_p at higher fields move quickly to low fields and finally merge into one peak, as shown in Fig. 5(a). In contrast to CVNS, there is only one maximum in the $f_p(h)$ curves for CVS-1 as shown in Fig. 5(b). The normalized pinning force can be approximately described by the formula of $f_p = h^{1.4}(1-h)^{1.8}$, which has a maximum of pinning force at the position of $h \sim 0.44$. This functional form is close to that for normal-core-pointlike pinning, $f_p = h(1-h)^2$, with a maximum at $h \sim 0.33$. The obtained h value in CVS-1 is very close to that in $BaFe_{1.8}Co_{0.2}As_2$ ($h \sim 0.45$) [56,57], which also suggested that pinning is probably due to weak pinning centers [56]. It should be noted that the f_p-h curves shown in Fig. 5(b) are dominated by the curves above H_{on}, indicating that the scaling function is characterizing the vortex state at high fields. One should also note that f_p does not seem to approach zero even at $h = 0$ as shown in Fig. 5(b). This is due to the fact that a single vortex regime, where J_c is independent of H, occurs only at very small fields ($h \ll 0.1$) in irradiated CVS.

It is well known that proton irradiation induces point defects in superconductors, which can act as pinning centers [58]. Thus it is reasonable that the peak effect in the CVS-1 is caused by the normal-core pinning [39]. If this scenario is correct, it is natural to expect a similar broad peak effect in CVNS-1. However, no peak effects are observed in CVNS-1. If the broad peak effect is originated from the normal-core pinning, as mentioned above, it should sensitively depend on the type, size, and density of pinning centers. For example, it has been observed that the level of disorder and/or defect density in $RbCa_2Fe_4As_4F_2$ has a significant effect on its second magnetization peak and J_c-H characteristics [59]. Furthermore, the fishtail effect is observed in KFe_2As_2 intercalated $CaKFe_4As_4$ but absent in $CaFe_2As_2$ intercalated ones [60]. The density and dimensions of irradiation-induced defects in CsV_3Sb_5 and $Cs(V_{0.93}Nb_{0.07})_3Sb_5$ after the proton irradiation should be similar at the same dose. Thus it is reasonable to deduce that the difference in the peak effect is originated from their different defect structures. Although direct observation of point defects generated by proton irradiation is challenging and has not been reported for CVS, their dimensions are believed to be smaller than typical diameters of columnar defects of 5–8 nm created by heavy-ion irradiation. On the other hand, the coherence lengths for CVS-1 and CVNS-1 at 2 K are about 19.5 and 19.1 nm, respectively. Thus point pinning centers generated by proton irradiation much smaller than the coherence length may not be effective. If point defects in CVS-1 are mobile under the help of thermal activation, they may agglomerate and form larger point defects with much stronger pinning and induce the peak effect in CVS-1. In addition, such agglomeration of point defects may be hindered by the presence of the impurity atom of Nb in CVNS-1. Alternatively, the enhanced pinning after the proton irradiation in CVS could be due to partial decomposition of the material triggered by the creation of point defects. In this case, the presence of Nb in CVNS may suppress such a decomposition process. Microstructural analyses using a transmission microscope may help to clarify the nature of point defects generated by proton irradiation including their possible evolution with time.

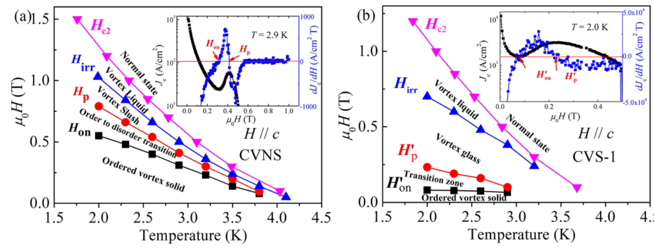

FIG. 6. The vortex phase diagrams for (a) CVNS and (b) CVS-1. Insets: illustration of the method to determine the values of H_{on} and H_p for CNVS and H'_{on} and H'_p for CVS-1 samples.

In Fig. 6, we present the vortex phase diagrams for CVNS and CVS-1. As mentioned above, H_{irr} and H_{c2} are the irreversibility field and the upper critical field, respectively. Above the $H_{c2}(T)$ line, both systems are in the normal state, and between the H_{irr} and H_{c2} lines, the systems change into the vortex liquid state, where vortices can move freely. For the CVNS, the system should be in the ordered vortex solid region below the H_{on} line. The vortex motion can be described by the mechanism of collective pinning of vortices [61]. With increasing applied magnetic field and/or temperature, the shear modulus C_{66} of the vortex lattice decreases. Thus, above the line of H_{on}, vortices begin to become disordered. During this process, vortices can be relaxed and occupy energetically favorable pinning centers, leading to the local maximum of pinning force at H_p. However, above H_p, vortices become much more mobile and the J_c rapidly drops to zero. Based on these analyses, a phase diagram of vortices has been drawn for CVNS as shown in Fig. 6(a). For CVS-1, the single vortex pinning becomes dominant below H'_{on}. In this region, vortices are pinned by sparse strong pinning centers. It usually shows high superconducting critical current density and large pinning energy. With increasing magnetic fields ($H'_{on} < H < H'_p$), more and more vortices are introduced and the number of strong pinning centers becomes much less than that of vortices. These additional vortices have to be pinned by weaker pinning centers and the collective pinning starts to control the motion of vortices. The change from strong pinning to weak collective pinning is accompanied by rapid suppression of J_c as shown in Fig. 4(d). At higher magnetic fields, the intervortex distance becomes small and the overlap of vortices is significant. On one hand, vortex-vortex interaction causes the decrease of pinning force due to the overlap of vortices. On the other hand, the shear modulus C_{66} becomes small and the vortex lattice can easily be deformed and better adapted to random pinning centers, which causes the increase of pinning energy. For CVS-1, the total pinning energy increases during the process; thus the peak effect is observed [62]. According to the present experimental results, the vortex phase diagram for CVS-1 is also given as shown in Fig. 6(b). Recently, Zhang *et al.* constructed the vortex phase diagram of kagome superconductor CsV_3Sb_5 in a temperature range between 0.12 and 4 K by using the ac mutual inductance technique. They also observed a peak effect in a broad intermediate range of magnetic fields. The peak effect is interpreted as a result of crossover from strong to weak pinning, which is consistent with the phase diagram of the present CVS-1 sample [48].

In summary, we have demonstrated that superconductivity of CsV_3Sb_5 single crystals can be enhanced by proton irradiation. Besides the enhanced J_c, the T_c is enhanced up to 4.4 K after proton irradiation at a dose of 0.1×10^{16} ions/cm^2. A clear broad peak effect has been found in proton-irradiated CsV_3Sb_5 single crystals. We also observe a peak effect very close to H_{c2} in the $Cs(V_{0.93}Nb_{0.07})_3Sb_5$ crystals, which can be attributed to the order-disorder transition of vortices. Finally, the vortex phase diagrams for CsV_3Sb_5 and $Cs(V_{0.93}Nb_{0.07})_3Sb_5$ with magnetic field parallel to the c axis have been constructed.

ACKNOWLEDGMENTS

This work has been supported by the China Scholarship Council (CSC), and the Natural Science Foundation of the Henan province of China (Grant No. 202300410342). The work at the Beijing Institute of Technology was supported by the National Natural Science Foundation of China (Grant No. 92065109), and the Beijing Natural Science Foundation (Grant No. Z210006).

[1] G. Ghiringhelli, M. L. E. Tacon, M. Minola, S. Blanco-Canosa, C. Mazzoli, N. B. Brookes, G. M. D. E. Luca, A. Frano, D. G. Hawthorn, F. He, T. Loew, M. Moretti Sala, D. C. Peets, M. Salluzzo, E. Schierle, R. Sutarto, G. A. Sawatzky, E. Weschke, B. Keimer, and L. Braicovich, Long-range incommensurate charge fluctuations in (Y,Nd)$Ba_2Cu_3O_{6+x}$, Science **337**, 821 (2012).

[2] A. J. Achkar, R. Sutarto, X. Mao, F. He, A. Frano, S. Blanco-Canosa, M. Le Tacon, G. Ghiringhelli, L. Braicovich, M. Minola, M. Moretti Sala, C. Mazzoli, R. Liang, D. A. Bonn, W. N. Hardy, B. Keimer, G. A. Sawatzky, and D. G. Hawthorn, Distinct charge orders in the planes and chains of ortho-III-ordered $YBa_2Cu_3O_{6+\delta}$ superconductors identified by resonant elastic x-ray scattering, Phys. Rev. Lett. **109**, 167001 (2012).

[3] P. Dai, Antiferromagnetic order and spin dynamics in iron-based superconductors, Rev. Mod. Phys. **87**, 855 (2015).

[4] H. Q. Luo, R. Zhang, M. Laver, Z. Yamani, M. Wang, X. Y. Lu, M. Y. Wang, Y. C. Chen, S. L. Li, S. Chang, J. W. Lynn, and P. C. Dai, Coexistence and competition of the short-range incommensurate antiferromagnetic order with the superconducting state of $BaFe_{2-x}Ni_xAs_2$, Phys. Rev. Lett. **108**, 247002 (2012).

[5] C. M. Varma, Phenomenological aspects of heavy fermions, Phys. Rev. Lett. **55**, 2723 (1985).

[6] P. W. Anderson, Heavy-electron superconductors, spin fluctuations, and triplet pairing, Phys. Rev. B **30**, 1549 (1984).

[7] B. R. Ortiz, L. C. Gomes, J. R. Morey, M. Winiarski, M. Bordelon, J. S. Mangum, I. W. H. Oswald, J. A. Rodriguez-Rivera, J. R. Neilson, S. D. Wilson, E. Ertekin, T. M. McQueen, and E. S. Toberer, New kagome prototype materials: Discovery of KV_3Sb_5, RbV_3Sb_5, and CsV_3Sb_5, Phys. Rev. Mater. **3**, 094407 (2019).

[8] Y. Luo, Y. L. Han, J. J. Liu, H. Chen, Z. H. Huang, L. W. Huai, H. Y. Li, B. Q. Wang, J. C. Shen, and S. H. Ding, A unique van Hove singularity in kagome superconductor $CsV_{3-x}Ta_xSb_5$ with enhanced superconductivity, Nat. Commun. **14**, 3819 (2023).

[9] X. X. Zhou, Y. K. Li, Z. Liu, J. H. Hao, Y. M. Dai, Z. W. Wang, Y. G. Yao, and H. H. Wen, Effects of niobium doping on the charge density wave and electronic correlations in the kagome metal $Cs(V_{1-x}Nb_x)_3Sb_5$, Phys. Rev. B **107**, 125124 (2023).

[10] S. L. Ni, S. Ma, Y. H. Zhang, J. Yuan, H. T. Yang, Z. Y. W. Lu, N. N. Wang, J. P. Sun, Z. Zhao, D. Li *et al.*, Anisotropic superconducting properties of kagome metal CsV_3Sb_5, Chin. Phys. Lett. **38**, 057403 (2021).

[11] Y. Xiang, Q. Li, Y. K. Li, W. Xie, H. Yang, Z. W. Wang, Y. G. Yao, and H. H. Wen, Twofold symmetry of c-axis resistivity in topological kagome superconductor CsV_3Sb_5 with in-plane rotating magnetic field, Nat. Commun. **12**, 6727 (2021).

[12] B. R. Ortiz, S. M. L. Teicher, Y. Lu, J. L. Zuo, P. M. Sarte, E. C. Schuller, A. M. M. Abeykoon, M. J. Krogstad, S. Rosenkranz, R. Osborn, R. Seshadri, L. Balents, J. F. He, and S. D. Wilson, CsV_3Sb_5: A Z_2 topological kagome metal with a superconducting ground state, Phys. Rev. Lett. **125**, 247002 (2020).

[13] S. Y. Yang, Y. J. Wang, B. R. Ortiz, D. F. Liu, J. Gayles, E. Derunova, R. Gonzalez-Hernandez, L. Šmejkal, Y. L. Chen, S. S. P. Parkin, S. D. Wilson, E. S. Toberer, T. Mcqueen, and M. N. Ali, Giant, unconventional anomalous Hall effect in the metallic frustrated magnet candidate, KV_3Sb_5, Sci. Adv. **6**, eabb6003 (2020).

[14] G. L. Zheng, C. Tan, Z. Chen, M. Y. Wang, X. D. Zhu, S. Albarakati, M. Algarni, J. Partridge, L. Farrar, J. H. Zhou, W. Ning, M. L. Tian, M. S. Fuhrer, and L. Wang, Electrically controlled superconductor-to-failed insulator transition and giant anomalous Hall effect in kagome metal CsV_3Sb_5 nanoflakes, Nat. Commun. **14**, 678 (2023).

[15] Y. P. Song, T. P. Ying, X. Chen, X. Han, X. X. Wu, A. P. Schnyder, Y. Huang, J. G. Guo, and X. L. Chen, Competition of superconductivity and charge density wave in selective oxidized CsV_3Sb_5 thin flakes, Phys. Rev. Lett. **127**, 237001 (2021).

[16] B. Q. Song, T. P. Ying, X. X. Wu, W. Xia, Q. W. Yin, Q. H. Zhang, Y. P. Song, X. F. Yang, J. G. Guo, L. Gu, X. L. Chen, J. P. Hu, A. P. Schnyder, H. C. Lei, Y. F. Guo, and S. Y. Li, Anomalous enhancement of charge density wave in kagome superconductor CsV_3Sb_5 approaching the 2D limit, Nat. Commun. **14**, 2492 (2023).

[17] Q. Wang, P. F. Kong, W. J. Shi, C. Y. Pei, C. H. P. Wen, L. L. Gao, Y. Zhao, Q. W. Yin, Y. S. Wu, G. Li, H. C. Lei, J. Li, Y. L. Chen, S. C. Yan, and Y. P. Qi, Charge density wave orders and enhanced superconductivity under pressure in the kagome metal CsV_3Sb_5, Adv. Mater. **33**, 2102813 (2021).

[18] Y. X. Jiang, J. X. Yin, M. M. Denner, N. Shumiya, B. R. Ortiz, G. Xu, Z. Guguchia, J. Y. He, M. S. Hossain, X. X. Liu, J. Ruff, L. Kautzsch, S. S. Zhang, G. Q. Chang, I. Belopolski, Q. Zhang, T. A. Cochran, D. Multer, M. Litskevich, Z. J. Cheng *et al.*, Unconventional chiral charge order in kagome superconductor KV_3Sb_5, Nat. Mater. **20**, 1353 (2021).

[19] K. Y. Chen, N. N. Wang, Q. W. Yin, Y. H. Gu, K. Jiang, Z. J. Tu, C. S. Gong, Y. Uwatko, J. P. Sun, H. C. Lei, J. P. Hu, and

J. G. Cheng, Double superconducting dome and triple enhancement of T_c in the kagome superconductor CsV_3Sb_5 under high pressure, Phys. Rev. Lett. **126**, 247001 (2021).

[20] Y. K. Li, Q. Li, X. W. Fan, J. J. Liu, Q. Feng, M. Liu, C. L. Wang, J. X. Yin, J. X. Duan, X. Li, Z. W. Wang, H. H. Wen, and Y. G. Yao, Tuning the competition between superconductivity and charge order in the kagome superconductor $Cs(V_{1-x}Nb_x)_3Sb_5$, Phys. Rev. B **105**, L180507 (2022).

[21] Y. M. Oey, B. R. Ortiz, F. Kaboudvand, J. Frassineti, E. Garcia, S. Sanna, V. F. Mitrovic, R. Seshadri, and S. D. Wilson, Fermi level tuning and double-dome superconductivity in the kagome metal $CsV_3Sb_{5-x}Sn_x$, Phys. Rev. Mater. **6**, L041801 (2022).

[22] H. Yang, Z. Huang, Y. Zhang, Z. Zhao, J. Shi, H. Luo, L. Zhao, G. Qian, H. Tan, B. Hu, K. Zhu, Z. Lu, H. Zhang, J. Sun, J. Cheng, C. Shen, X. Lin, B. Yan, X. Zhou, Z. Wang *et al.*, Titanium doped kagome superconductor $CsV_{3-x}Ti_xSb_5$ and two distinct phases, Sci. Bull. **67**, 2176 (2022).

[23] L. Kautzsch, Y. M. Oey, H. Li, Z. Ren, B. R. Ortiz, G. Pokharel, R. Seshadri, J. Ruff, T. Kongruengkit, J. W. Harter, Z. Q. Wang, I. Zeljkovic, and S. D. Wilson, Incommensurate charge-stripe correlations in the kagome superconductor $CsV_3Sb_{5-x}Sn_x$, npj Quantum Mater. **8**, 37 (2023).

[24] W. J. Li, S. S. Pyon, A. Yagi, T. Ren, M. Suyama, J. Wang, T. Matsumae, Y. Kobayashi, A. Takahashi, D. Miyawaki, and T. Tamegai, Effects of 3 MeV proton irradiation on superconductivity and CDW in $2H$-$NbSe_2$ single crystals, J. Phys. Soc. Jpn. **92**, 064701 (2023).

[25] M. Roppongi, K. Ishihara, Y. Tanaka, K. Ogawa, K. Okada, S. Liu, K. Mukasa, Y. Mizukami, Y. Uwatoko, R. Grasset, M. Konczykowski, B. R. Ortiz, S. D. Wilson, K. Hashimoto, and T. Shibauchi, Bulk evidence of anisotropic *s*-wave pairing with no sign change in the kagome superconductor CsV_3Sb_5, Nat. Commun. **14**, 667 (2023).

[26] T. Taen, F. Ohtake, H. Akiyama, H. Inoue, Y. Sun, S. Pyon, T. Tamegai, and H. Kitamura, Pair-breaking effects induced by 3-MeV proton irradiation in $Ba_{1-x}K_xFe_2As_2$, Phys. Rev. B **88**, 224514 (2013).

[27] C. Tarantini, M. Putti, A. Gurevich, Y. Shen, R. K. Singh, J. M. Rowell, N. Newman, D. C. Larbalestier, P. Cheng, Y. Jia, and H.-H. Wen, Suppression of the critical temperature of superconducting NdFeAs(OF) single crystals by Kondo-like defect sites induced by α-particle irradiation, Phys. Rev. Lett. **104**, 087002 (2010).

[28] Y. Nakajima, T. Taen, Y. Tsuchiya, T. Tamegai, H. Kitamura, and T. Murakami, Suppression of the critical temperature of superconducting $Ba(Fe_{1-x}Co_x)_2As_2$ by point defects from proton irradiation, Phy. Rev. B **82**, 220504(R) (2010).

[29] K. Cho, M. Konczykowski, S. Teknowijoyo, M. A. Tanatar, J. Guss, P. Gartin, J. M. Wilde, A. Kreyssig, R. McQueeney, A. I. Goldman, V. Mishra, P. J. Hirschfeld, and R. Prozorov, Using controlled disorder to probe the interplay between charge order and superconductivity in $NbSe_2$, Nat. Commun. **9**, 2796 (2018).

[30] M. Leroux, V. Mishra, C. Opagiste, P. Rodière, A. Kayani, W. Kwok, and U. Welp, Charge density wave and superconductivity competition in $Lu_5Ir_4Si_{10}$: A proton irradiation study, Phys. Rev. B **102**, 094519 (2020).

[31] S. L. Li, H. H. Wen, Z. W. Zhao, Y. M. Ni, Z. A. Ren, G. C. Che, H. P. Yang, Z. Y. Liu, and Z. X. Zhao, Linear temperature dependence of lower critical field in MgB_2, Phys. Rev. B **64**, 094522 (2001).

[32] L. Shan, Y. L. Wang, B. Shen, B. Zeng, Y. Huang, A. Li, D. Wang, H. Yang, C. Ren, Q. H. Wang, S. H. Pan, and H. H. Wen, Observation of ordered vortices with Andreev bound states in $Ba_{0.6}K_{0.4}Fe_2As_2$, Nat. Phys. **7**, 325 (2011).

[33] A. Almoalem, A. Yagil, K. Cho, S. Teknowijoyo, M. A. Tanatar, R. Prozorov, Y. Liu, T. A. Lograsso, and O. M. Auslaender, Dependence of the absolute value of the penetration depth in $(Ba_{1-x}K_x)Fe_2As_2$ on doping, Phys. Rev. B **98**, 054516 (2018).

[34] J. Y. L. Li, W. Xie, J. J. Liu, Q. Li, X. Li, H. Yang, Z. W. Wang, Y. G. Yao, and H. H. Wen, Strong-coupling superconductivity and weak vortex pinning in Ta-doped CsV_3Sb_5 single crystals, Phys. Rev. B **106**, 214529 (2022).

[35] N. Kokubo, K. Kadowaki, and K. Takita, Peak effect and dynamic melting of vortex matter in $NbSe_2$ crystals, Phys. Rev. Lett. **95**, 177005 (2005).

[36] Y. J. Jiao, W. Cheng, Q. Deng, H. Yang, and H. H. Wen, Collective vortex pinning and merging of the irreversibility line and second peak effect in optimally doped BaK_xBiO_3 single crystals, Phys. C (Amsterdam) **545**, 43 (2018).

[37] T. Nishizaki, T. Naito, and N. Kobayashi, Anomalous magnetization and field-driven disordering transition of a vortex lattice in untwinned $YBa_2Cu_3O_y$, Phys. Rev. B **58**, 11169 (1998).

[38] J. Ziegler, J. Biersack, and U. Littmark, *The Stopping and Range of Ions in Solids* (Pergamon, New York, 1985), p. 202.

[39] T. Taen, F. Ohtake, S. Pyon, T. Tamegai, and H. Kitamura, Critical current density and vortex dynamics in pristine and proton-irradiated $Ba_{0.6}K_{0.4}Fe_2As_2$, Supercond. Sci. Technol. **28**, 085003 (2015).

[40] K. J. Kihlstrom, L. Fang, Y. Jia, B. Shen, A. E. Koshelev, U. Welp, G. W. Crabtree, W. K. Kwok, A. Kayani, S. F. Zhu, and H. H. Wen, High-field critical current enhancement by irradiation induced correlated and random defects in $(Ba_{0.6}K_{0.4})Fe_2As_2$, Appl. Phys. Lett. **103**, 202601 (2013).

[41] H. H. Wen, Superconducting gap opens fully in the newly found topological kagome metal CsV_3Sb_5, Sci. China Phys. Mech. **64**, 107463 (2021).

[42] See Supplemental Material at http://link.aps.org/supplemental/10.1103/PhysRevB.109.024514 for the data on the temperature dependence of normalized resistivity, magnetization hysteresis loops, the magnetic fields dependence of relaxation ratio (Q) and critical current density (J_c).

[43] H. Q. Luo, Z. S. Wang, H. Yang, P. Cheng, X. Y. Zhu, and H. H. Wen, Growth and characterization of $A_{1-x}K_xFe_2As_2$ (A = Ba, Sr) single crystals with $x = 0$–0.4, Supercond. Sci. Technol. **21**, 125014 (2008).

[44] X. L. Wang, A. H. Li, S. Yu, S. Ooi, K. Hirata, C. T. Lin, E. W. Collings, M. D. Sumption, M. Bhatia, S. Y. Ding, and S. X. Dou, Thermally assisted flux flow and individual vortex pinning in $Bi_2Sr_2Ca_2Cu_3O_{10}$ single crystals grown by the traveling solvent floating zone technique, J. Appl. Phys. **97**, 10B114 (2005).

[45] J. Jaroszynski, F. Hunte, L. Balicas, Y.-j. Jo, I. Raičević, A. Gurevich, D. C. Larbalestier, F. F. Balakirev, L. Fang, P. Cheng, Y. Jia, and H. H. Wen, Upper critical fields and thermally-activated transport of $NdFeAsO_{0.7}F_{0.3}$ single crystal, Phys. Rev. B **78**, 174523 (2008).

[46] D. Li, P. P. Shen, J. P. Tian, G. He, S. L. Ni, Z. S. Wang, C. Y. Xi, L. Pi, H. Zhang, J. Yuan, K. Jin, E. F. Talantsev, L. Yu, F. Zhou, J. Hänisch, X. L. Dong, and Z. X. Zhao, A disorder-sensitive emergent vortex phase indentified in high-T_c superconductor (Li,Fe)OHFeSe, Supercond. Sci. Technol. **35**, 064007 (2022).

[47] H. S. Xu, Y. J. Yan, R. Yin, W. Xia, S. Fang, Z. Chen, Y. Li, W. Yang, Y. Guo, and D. L. Feng, Multiband superconductivity with sign-preserving order parameter in kagome superconductor CsV_3Sb_5, Phys. Rev. Lett. **127**, 187004 (2021).

[48] X. Y. Zhang, M. Zic, D. Chen, C. Shekhar, C. Felser, I. R. Fisher, and A. Kapitulnik, Vortex phase diagram of kagome superconductor CsV_3Sb_5, arXiv:2306.13297.

[49] S. S. Banerjee, S. Saha, N. G. Patil, S. Ramakrishnan, A. K. Grover, S. Bhattacharya, G. Ravikumar, P. K. Mishra, T. V. C. Rao, V. C. Sahni, C. V. Tomy, G. Balakrishnan, D. Mck. Paul, and M. J. Higgins, Generic phase diagram for vortex matter via a study of peak effect phenomenon in crystals of 2H-$NbSe_2$, Phys. C (Amsterdam) **308**, 25 (1998).

[50] D. Larbalestier, A. Gurevich, D. Feldmann, and A. Polyanskii, High-T_c superconducting materials for electric power applications, Nature (London) **414**, 368 (2001).

[51] G. Blatter, M. V. Feigel'man, V. B. Geshkenbein, A. I. Larkin, and V. M. Vinokur, Vortices in high-temperature superconductors, Rev. Mod. Phys. **66**, 1125 (1994).

[52] U. Welp, W. K. Kwok, G. W. Crabtree, K. G. Vandervoort, and J. Z. Liu, Magnetization hysteresis and flux pinning in twinned and untwinned $YBa_2Cu_3O_{7-\delta}$ single crystals, Appl. Phys. Lett. **57**, 84 (1990).

[53] H. Yang, H. Q. Luo, Z. S. Wang, and H. H. Wen, Fishtail effect and the vortex phase diagram of single crystal $Ba_{0.6}K_{0.4}Fe_2As_2$, Appl. Phys Lett. **93**, 142506 (2008).

[54] L. M. Wang, U.-C. Sou, H. C. Yang, L. J. Chang, C. M. Cheng, K. D. Tsuei, Y. Su, Th. Wolf, and P. Adelmenn, Mixed-state Hall effect and flux pinning in $Ba(Fe_{1-x}Co_x)_2As_2$ single crystals ($x = 0.08$ and 0.10), Phys. Rev. B **83**, 134506 (2011).

[55] C. L. Wang, T. He, Q. Q. Han, C. F. Fan, Q. B. Tang, D. Chen, Q. K. Lei, S. J. Sun, Y. B. Li, and B. H. Yu, Novel sample-thickness-dependent flux pinning behaviors of KFe_2As_2 intercalations in $CaKFe_4As_4$ single crystals, Supercond. Sci. Technol. **34**, 055001 (2022).

[56] D. L. Sun, Y. Liu, and C. T. Lin, Comparative study of upper critical field H_{c2} and second magnetization peak H_{sp} in hole- and electron-doped $BaFe_2As_2$ superconductors, Phys. Rev. B **80**, 144515 (2009).

[57] A. Yamamoto, J. Jaroszynski, C. Tarantini, L. Balicas, J. Jiang, A. Gurevich, D. C. Larbalestier, R. Jin, A. S. Sefat, M. A. McGuire, B. C. Sales, D. K. Christen, and D. Mandrus, Small anisotropy, weak thermal fluctuations, and high field superconductivity in Co-doped iron pnictide $Ba(Fe_{1-x}Co_x)_2As_2$, Appl. Phys. Lett. **94**, 062511 (2009).

[58] A. Park, A. Mine, T. Yamada, F. Ohtake, H. Akiyama, Y. Sun, S. Pyon, T. Tamegai, Y. Kitahama, T. Mizukami, K. Kudo, M. Nohara, and H. Kitamura, Enhancement of critical current density in a $Ca_{0.85}La_{0.15}Fe(As_{0.92}Sb_{0.08})_2$ superconductor with $T_c = 47$ K through 3 MeV proton irradiation, Supercond. Sci. Technol. **29**, 055006 (2016).

[59] X. L. Yi, X. Z. Xing, Y. Meng, N. Zhou, C. L. Wang, Y. Sun, and Z. X. Shi, Anomalous second magnetization peak in 12442-type $RbCa_2Fe_4As_4F_2$ superconductors, Chin. Phys. Lett. **40**, 027401 (2023).

[60] C. L. Wang, T. He, D. Chen, J. Y. Zhang, C. F. Fan, Q. B. Tang, C. H. Dong, Y. C. Tu, B. H. Yi, and Y. W. Ma, From δl- to δT_c-pinning in $CaKFe_4As_4$ single crystals obtained by adjusting their defect structures, Supercond. Sci. Technol. **34**, 115020 (2021).

[61] A. M. Campbell and J. E. Evetts, Flux vortices and transport currents in type II superconductor, Adv. Phys. **21**, 199 (1972).

[62] X. Z. Xing, Z. F. Li, I. Veshchunov, X. L. Yi, Y. Meng, M. Li, B. C. Lin, T. Tamegai, and Z. X. Shi, Reemergence of superconductivity by 4d transition-metal Pd doping in over-doped 112-type iron pnictide superconductors $Ca_{0.755}La_{0.245}FeAs_2$, New J. Phys. **21**, 093015 (2019).